VARIATION OF TURBULENCE IN THE MARINE BOUNDARY LAYER OVER THE ARABIAN SEA DURING INDIAN SOUTHWEST MONSOON (MONEX 79)

TEDDY HOLT and SETHU RAMAN

Department of Marine, Earth and Atmospheric Sciences, North Carolina State University, Raleigh, NC 27695–8208, U.S.A.

(Received in final form 23 April, 1986)

Abstract. Analysis of high frequency (20 Hz) turbulence data collected from low level flights by the National Center for Atmospheric Research (NCAR) Electra aircraft over the central Arabian Sea on 20 and 24 June, 1979 as part of MONEX 79 indicates the influence of the Somali Jet on boundary-layer turbulence. Different stages of monsoon development were evident on the two observation days from mean boundary-layer profiles. However, turbulence statistics of wind speed components and temperature in the monsoon boundary layer for both days are generally greater than those observed in laboratory experiments or tropical and trade wind boundary layers in which a strong jet was not present. Analysis of high frequency wind, temperature and humidity data was made to obtain fluxes of momentum and heat. Magnitudes of the sensible and latent heat fluxes are three to five times larger than the values observed over the monsoon boundary layer over the Bay of Bengal. The turbulent kinetic energy budget over the Arabian Sea for 24 June indicates the importance of buoyancy, and to a lesser extent shear as the dominant term. Dissipation serves as the primary sink term.

1. Introduction

The Indian southwest monsoon is characterized by a strong northward cross-equatorial flow of moist air off the eastern coast of Africa as indicated in several studies (e.g., Saha and Bavadekar, 1973; Cadet and Reverdin, 1981) along with a prevalent low-level jet over the Arabian Sea whose roots originate in the Masacarene High and Mozambique Channel (Findlater, 1969; van de Boogaard and Rao, 1984). The core of this Somali Jet as it crosses the equator with strong, moist southerly flow is typically situated at altitudes approximately 1.5 to 2.0 km over East Africa. Usual separation from the African coast seems to occur at about 10° N with a wind speed maximum at about 1 km height to the northeast of the tip of the Horn of Somalia. With boundary-layer depths over the Arabian Sea generally observed to be on the order of 1 km, the Somali Jet would appear to play an important role in the dynamics of the monsoon boundary layer.

The purpose of this paper is to examine the turbulence structure of the monsoon boundary layer over the Arabian Sea during the advance of the 1979 southwest monsoon, using data obtained during MONEX 79. Mean structure of the monsoon boundary layer was the subject of an earlier paper (Holt and SethuRaman, 1985). Emphasis in this paper is placed on understanding the impact of the Somali Jet on turbulence statistics in the marine boundary layer over the Arabian Sea. The study area is divided into four regions (north, south, east, and west) because of significant differences in the convection patterns.

Boundary-Layer Meteorology 37 (1986) 71–87.

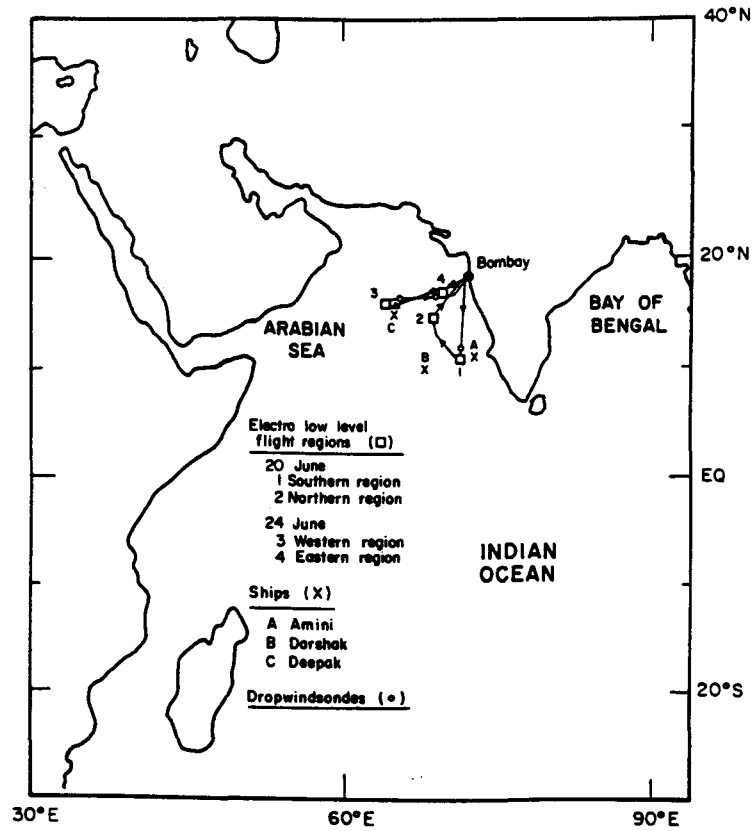

Fig. 1. Arabian Sea regions sampled by the Electra, ships, and dropwindsondes for 20 and 24 June, 1979. Solid lines indicate flight tracks. The northern-most flight track flown roughly east–west is for 24 June while that to the south is for 20 June. Boxes show areas of low-level aircraft stepped legs of primary interest in this study.

2. Data and Analysis

A variety of observation platforms were used during MONEX 79 to collect boundary-layer data over the monsoon region shown in Figure 1. During the summer phase of MONEX 79 over the Arabian Sea, the NCAR Electra flew 14 sorties from the period 29 May–4 July out of Bombay, India (Bolhofer *et al.*, 1981). Flight tracks and low-level flight regions in which stepped legs were flown for the two observation days over the Arabian Sea considered in this study, 20 June and 24 June, are also given in Figure 1 along with dropwindsonde locations and ship positions. The flight mission on 20 June was designed to study heat sources and sinks over the central Arabian Sea and was also a dropwindsonde mission. The 24 June flight was intended as a detailed investigation of the low-level Somali Jet in the regions east of the northeast African coast. A primary objective was to study the low level flow with vertical profiling and dropwindsondes. Low-level flight data from the gust probe system of the Electra for the four regions on 20 June and 24 June (Figure 1) consisted of both low (1 Hz) and high (20 Hz) frequency

fluctuations of components of wind speed, ambient temperature and specific humidity for altitudes from approximately 80 to 700 m. Four boundary-layer legs at various altitudes were flown over each region, the time of each leg being about 8 min. Low-frequency measurements were used primarily as a means of quality control. Time series analysis of each variable was performed for each altitude when the records were of sufficient length to obtain statistically meaningful results. Data were further edited to eliminate spurious spikes which were of the order of 0.2% scattered at random. Mean, standard deviation and range of each variable were also obtained using standard statistical procedures. Flux analysis involved only the high frequency (20 Hz) data and consisted of a single cross-covariance analysis of two time series.

From the pressure, temperature and moisture data, mean values of virtual potential temperature (θ_V) and equivalent potential temperature (θ_E) are obtained:

$$\theta_V = T_V \left(\frac{1000}{p}\right)^{2/7}, \tag{1}$$

$$\theta_E = \theta \exp(L_V r / c_p T_{\mathrm{LCL}}) \tag{2}$$

where the temperature at the lifted condensation level $T_{\mathrm{LCL}} = T_d - (0.001296 T_d + 0.1963)(T - T_d)$, and L_V is the latent heat of vaporization, r the mixing ratio and c_p the specific heat (Barnes, 1968). Spectral analysis was performed using Fast Fourier Transform (FFT) techniques to estimate the energy dissipation rate ε of the turbulent kinetic energy. The dissipation rate was then obtained from the inertial subrange of the longitudinal velocity spectra using a Kolmogorov constant of 0.67 (Lenschow *et al.*, 1980). Scaling parameters such as u_*, the friction velocity, w_*, the convective velocity, θ_*, the convective temperature and L, the Monin–Obukhov length were calculated from:

$$u_* = [(\overline{u'w'})_0^2 + (\overline{v'w'})_0^2]^{1/4}, \tag{3}$$

$$w_* = \left[\frac{g}{T} h(\overline{w'T_v'})_0\right]^{1/3}, \tag{4}$$

$$\theta_* = \frac{(\overline{w'T_v'})_0}{w_*}, \tag{5}$$

$$L = -\frac{\overline{T}_v u_*^3}{kg(\overline{w'T_v'})_0}, \tag{6}$$

where h is the mixed-layer depth estimated as the height of the lowest inversion base, T_v the virtual temperature, k von Karman's constant (0.4), and g the gravitational acceleration. Primes denote turbulent quantities and overbars indicate a mean value taken over the length of the flight leg. Surface fluxes were derived from estimates obtained by extrapolating observed flux profiles to the surface and agree well with values

TABLE I

Boundary-layer parameters over the Arabian Sea

	h (m)	L (m)	w_* (ms^{-1})	u_* (ms^{-1})	θ_* (°C)
20 June, 1979					
Southern region	1000	−227	0.735	0.330	0.0165
Northern region	800	−301	1.05	0.557	0.0419
24 June, 1979					
Western region	800	−1473	0.990	0.894	0.0375
Eastern region	600	−434	0.714	0.473	0.0261

obtained from bulk methods. Table I gives values of the above parameters for the four regions over the Arabian Sea sampled by the Electra on 20 June and 24 June, 1979.

Research vessels in the observational area on 20 June were the Indian ships Amini (11.0° N, 73.0° E) and Deepak (15.0° N, 65.0° E). Two Indian ships, Darshak (9.0° N, 68.0° E) and Deepak (15.0° N, 65.0° E) provided boundary-layer data for 24 June over the Arabian Sea. Each ship made observations every 6 hr of pressure, height, dry bulb and dew point temperatures and winds at the surface. They also launched radiosondes every 6 hr to obtain vertical profiles with a resolution of 50 mb. Dropwindsondes from the NCAR Electra were made at strategic locations along the flight track to obtain pressure, temperature, dew point depression and wind speed soundings. Synoptic weather maps provided information concerning the location and movement of large-scale systems affecting the boundary-layer processes.

3. Large-Scale Flow

The two observation days over the Arabian Sea during MONEX 79 studied here (20 and 24 June) are examples of different stages of monsoon flow as evident in the series of sea level pressure maps given in Figure 2. Shown are the 0000 GMT fields for the period 19–24 June with regions of boundary-layer observations for 20 and 24 June (Figures 2(b, f)) indicated by boxes. The area of observation for 20 June was slightly southeast of that for 24 June. A weakened tropical storm, first evident on 1 June, was located at approximately 19° N, 57° E near the Oman coast on 19 June (Figure 2(a)); by 22 June the storm dissipated. Associated with this storm was strong southwest monsoon low-level flow over the Arabian Sea which had reached approximately 8° N on 19 June (Sikka and Grossman, 1980). By 20 June, the strong monsoon flow had advanced into, but not completely covered, the observation region (box in Figure 2(b)). Along the western Indian coast, strong convective activity and heavy rainfall were observed.

The sea level pressure maps for the period 21–23 June (Figures 2(c–e)) further emphasize the strengthening of the low-level southwest monsoon flow and the

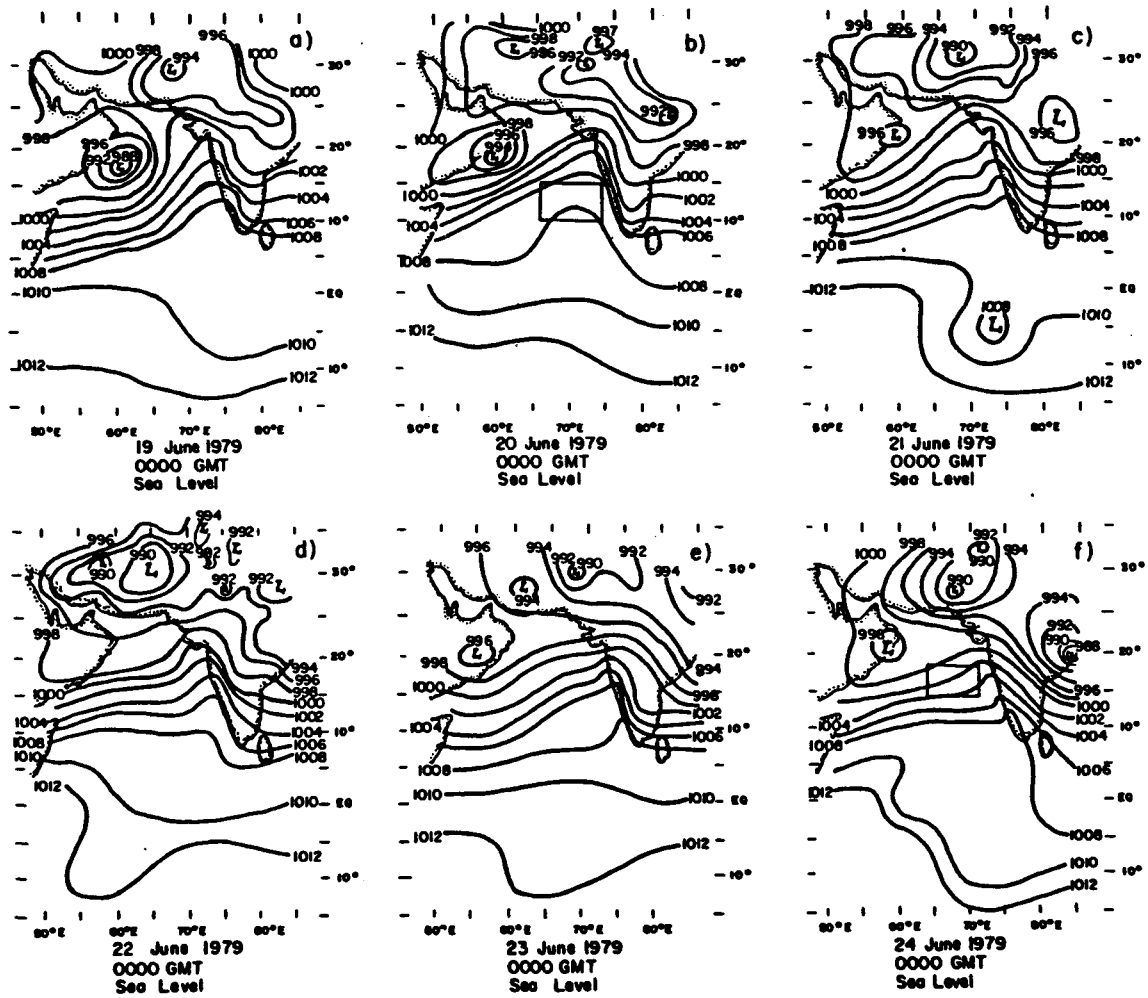

Fig. 2. Sea level pressure maps for 0000 GMT for the period 19–24 June, 1979 indicating the advance of the southwest monsoon. Boxes shown for 20 and 24 June indicate areas of boundary-layer observations.

northeastward advance of the monsoon. Intensification of the pressure gradient in the region from the tip of Somalia to the central Arabian Sea during this period signals the surge of the well-known Somali Jet (Bannon, 1982; Findlater, 1977). By 24 June, flow is from a more westsouthwest direction over the Arabian Sea with a large monsoon depression situated at the head of the Bay of Bengal (20° N, 85° E). A well-developed monsoon trough is present with most of India under massive cloudiness with strong convective activity along both coasts. Important differences are evident for the two observation regions on 20 June (box in Figure 2(b)) and 24 June (Figure 2(f)). Monsoon flow has not completely covered the region shown for 20 June with a much weaker pressure gradient evident than observed for 24 June. Strong southwesterly monsoon flow did not cover the entire Arabian Sea area until 22 June (Sikka and Grossman, 1980). Thus, the large-scale monsoon flow for 20 June can be considered as developing

flow while that on 24 June shows well-developed monsoon conditions. These differences in monsoon conditions will become more evident upon discussion of mean and turbulence profiles for the two days.

4. Mean Structure

To understand the variation of the turbulence in the boundary layer, some knowledge of the mean wind, temperature, and humidity profiles is needed. Discussion of vertical profiles of mean virtual potential temperature θ_v, mean equivalent potential temperature θ_E and mean resultant wind speed for the four observation regions on 20 and 24 June shown in Figure 1 are given in a separate paper (Holt and SethuRaman, 1985). Profiles for the Western Arabian Sea region on 24 June are shown here (Figure 3). The mean θ_v profile over the Western region (16.5° N, 63.9° E) shows a near-neutral profile up to approximately 800 m suggesting considerable mixing in the subcloud layer. The strong capping stable layer evident aloft between 920 and 700 mb delineates the height of the boundary layer. The mean θ_E profile indicates a very weak, conditionally unstable layer from near surface to 700 mb. The mean resultant wind speed profile over the Western region on 24 June shows a jet depressed in height with a maximum speed of approximately 22 ms^{-1} located roughly at the height of the boundary layer. In comparison, the mean profiles of θ_v, θ_E and wind speed for the Eastern region on 24 June (17.2° N, 69.9° E) (not shown here) indicate a much more shallow mixed layer (600 m) with the strong capping stable layer not evident until approximately 1500 m (Holt and SethuRaman, 1985). A near-neutral layer existed between 600–1500 m, suggesting multiple cloud layers. Aircraft observers' reports agree with these results and also indicate lowest cloud bases at approximately 600 m. The wind speed profile over the Eastern region shows a very deep, flat jet extending to a height of about 1600 m with maximum speeds of about 15 ms^{-1} at heights from 600 to 1500 m. Thus, the 24 June aircraft mission to study the low-level Somali Jet reveals significant differences in jet structure for the two regions separated approximately 650 km along the flow streamline.

The two regions (Southern and Northern) studied on 20 June also show important differences in the mean structure. The mean θ_v profile over the Southern Arabian Sea region (10.8° N, 71.2° E) (not shown here) indicates a stable layer from near the surface (100 m) to about 1000 m, indicating little convective mixing in the lower levels. A strong capping stable layer indicating the height of the boundary layer (1000 m) is observed from approximately 900 to 700 mb. The height of maximum wind speed over the Southern region agrees roughly with the height of the capping stable layer. In general, characteristics and profiles of the boundary layer over the Southern region on 20 June compare best with those of the Eastern region on 24 June. Likewise the boundary layer over the Northern region on 20 June (14.8° N, 69.0° E) is very similar to that of the Western region on 24 June. The mean θ_v profile for the Northern region shows a well mixed near-neutral layer from 100 to 800 m with a strong capping layer aloft. The mean wind speed profile for the Northern region shows a jet depressed in height similar to Figure 3 with a maximum speed of about 22 ms^{-1} at 700 m.

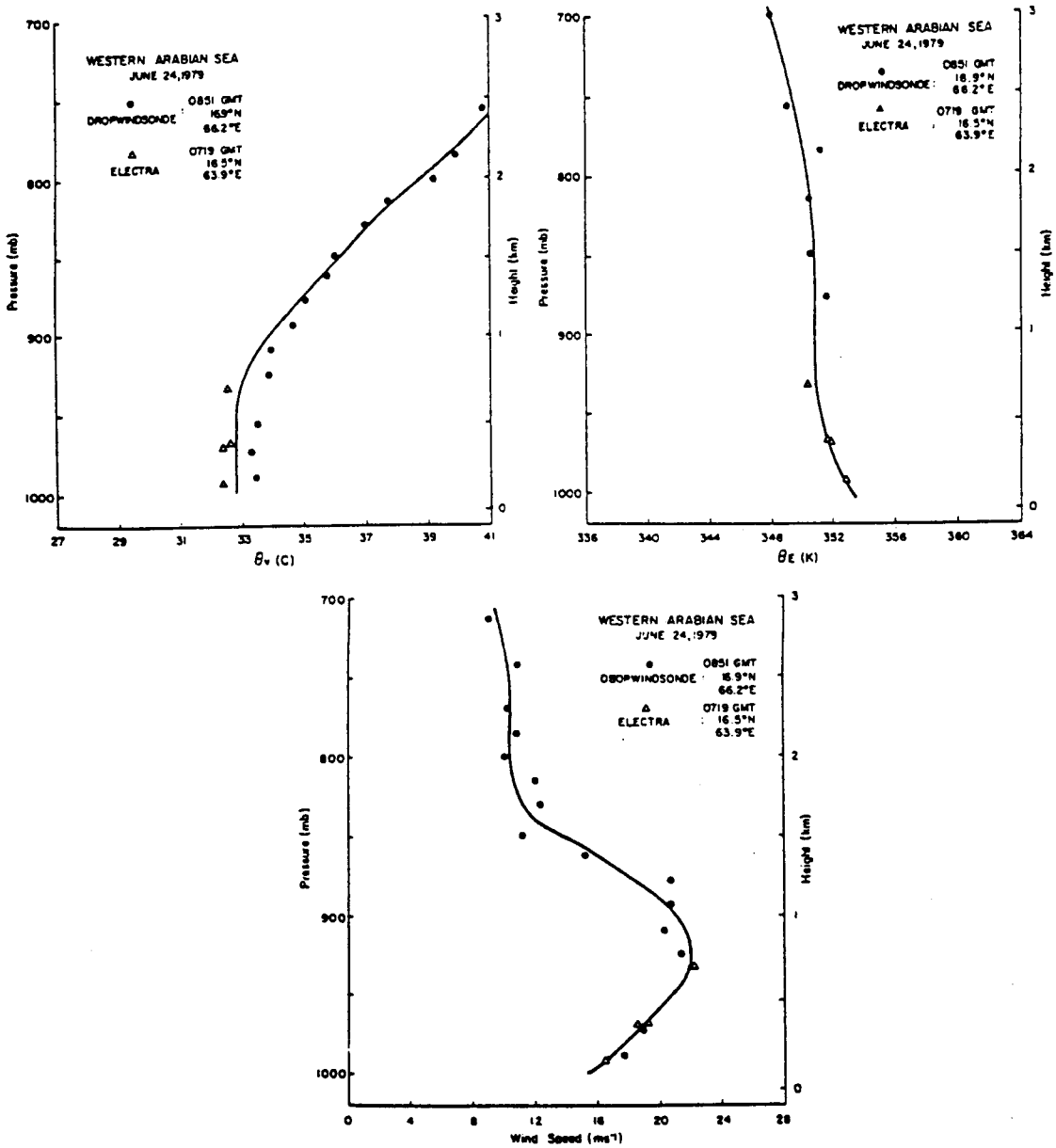

Fig. 3. Vertical profiles of mean virtual potential temperature θ_v, mean equivalent potential temperature θ_E and mean resultant wind speed for the Western Arabian Sea region on 24 June obtained from dropwindsonde and low-level Electra observations.

5. Flux and Turbulence Profiles

High-frequency data of wind components (u, v, w), temperature (T), and specific humidity (q) sampled at a rate of 20 s^{-1} during the NCAR Electra's flight over the Arabian Sea on 20 June and 24 June were used in turbulent flux computations.

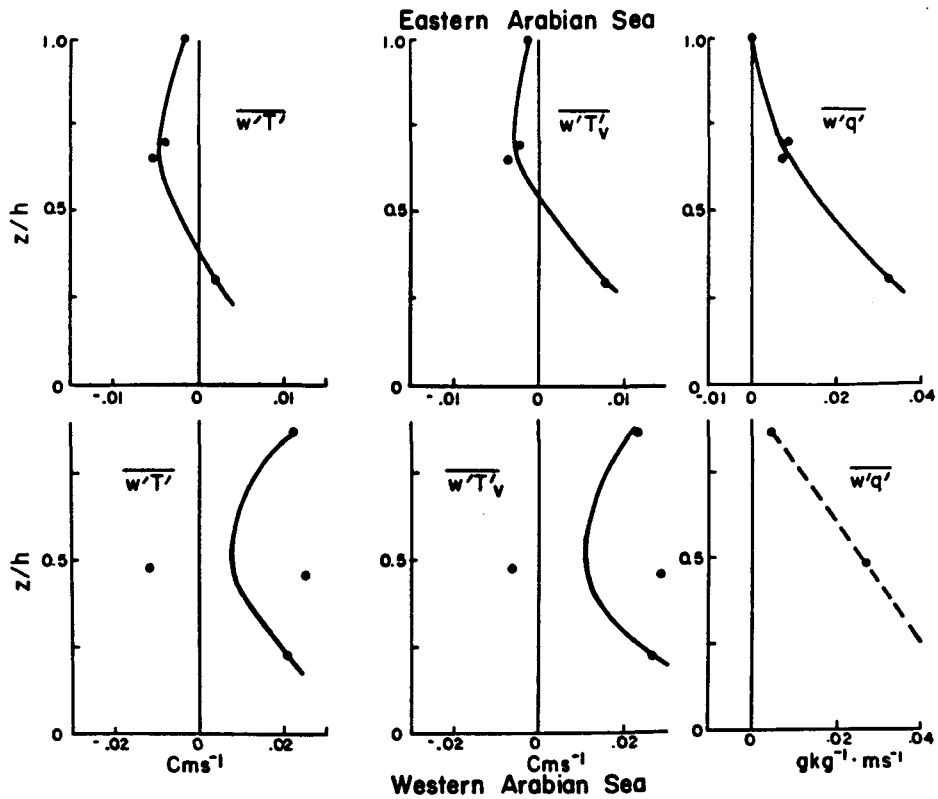

Fig. 4. Vertical variation of sensible heat flux $\overline{w'T'}$, virtual heat flux $\overline{w'T'_v}$ and latent heat flux $\overline{w'q'}$ for the Eastern and Western Arabian Sea regions on 24 June, 1979. Lines are drawn as eye averages.

Approximately 85% of the turbulence data collected over the two regions of the observations days were used in flux calculations. Humidity values proved to be the least reliable. Approximately 25% of the latent heat flux ($\overline{w'q'}$) boundary-layer data in the selected regions used in this study were spurious and had to be dropped. The data from the Northern Arabian Sea region on 20 June and the Western Arabian Sea region on 24 June were particularly bad. Interestingly, these two regions were areas of greater cloud and convective activity than generally observed over the Eastern or Southern regions.

Variation of turbulent latent and sensible heat fluxes and virtual heat flux for 24 June against normalized height z/h (Figure 4) are consistent with the observations of the mean structure of the boundary layer (Holt and SethuRaman, 1985). Mean profiles of θ_v and θ_E discussed in Section 4 over the Eastern Arabian Sea on 24 June indicate weak low-level instability from near the surface up to about 1 km. Suppressed convection and multiple cloud layers associated with a nearby congestus area are also evident (Grossman and Durran, 1984). Turbulent heat flux profiles for this region indicate a surface virtual heat flux of about 0.0186 ms^{-1} C with negative flux from $z = 0.5h$ to the top of the boundary layer. Sensible heat flux $\overline{w'T'}$ changes sign from positive to negative

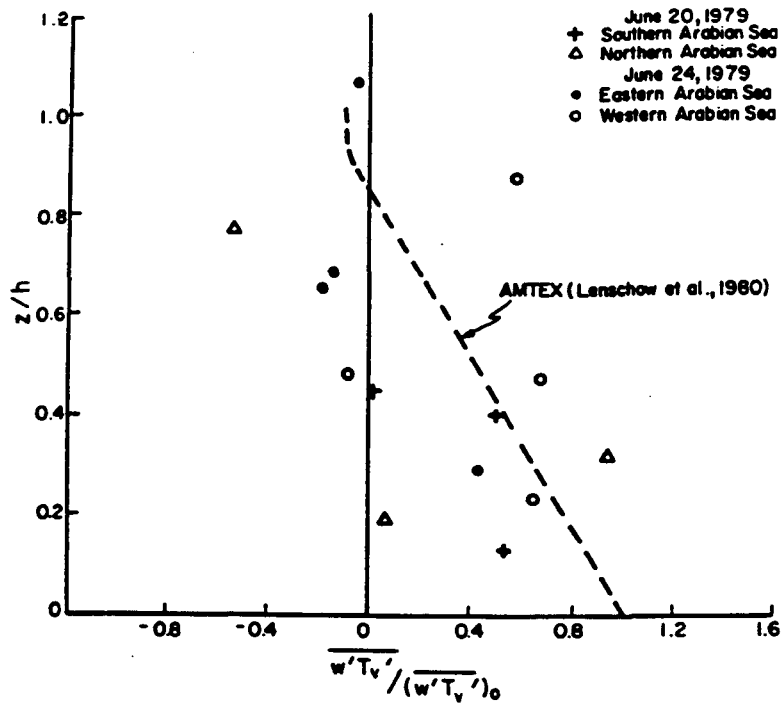

Fig. 5. Vertical variation of normalized virtual heat flux for all four observation regions (20 and 24 June). Dashed line is from AMTEX data (Lenschow *et al.*, 1980).

at a height of about $z = 0.25h$ (approximately 200 m). Nicholls and LeMone (1980) observed a change of sign at $z = 200$ m in an undisturbed tropical boundary layer during GATE. However, they observed that water vapor flux served to provide all the positive buoyancy in the upper half of the mixed layer. This is not observed over the Eastern Arabian Sea region. Water vapor flux approaches zero near the top of the boundary layer.

Flux profiles for the Western region indicate substantial virtual and sensible heat flux (0.01 to 0.02 ms^{-1} C) throughout the boundary layer, supporting mean observations of a near-neutral boundary layer. Fluxes do not show the expected linear decrease as observed over the Eastern region but indicate values at the top of the boundary layer roughly equal to that near the surface. This is probably because of stratocumulus convective clouds.

Figure 5 shows the vertical variation of virtual heat flux $\overline{w'T_v'}$ normalized by its surface value. Included are values from all four regions. The dashed line represents the profile obtained from Lenschow *et al.* (1980) using AMTEX data. Values observed over the Arabian Sea are generally smaller than those observed during AMTEX. More negative values of $\overline{w'T_v'}/(\overline{w'T_v'})_0$ occur above $z = 0.5h$, indicating possible cloud effects.

Figure 6 shows the variation of the standard deviation of vertical velocity fluctuations, σ_w normalized by w_* against the normalized height z/h for both 20 June and 24 June.

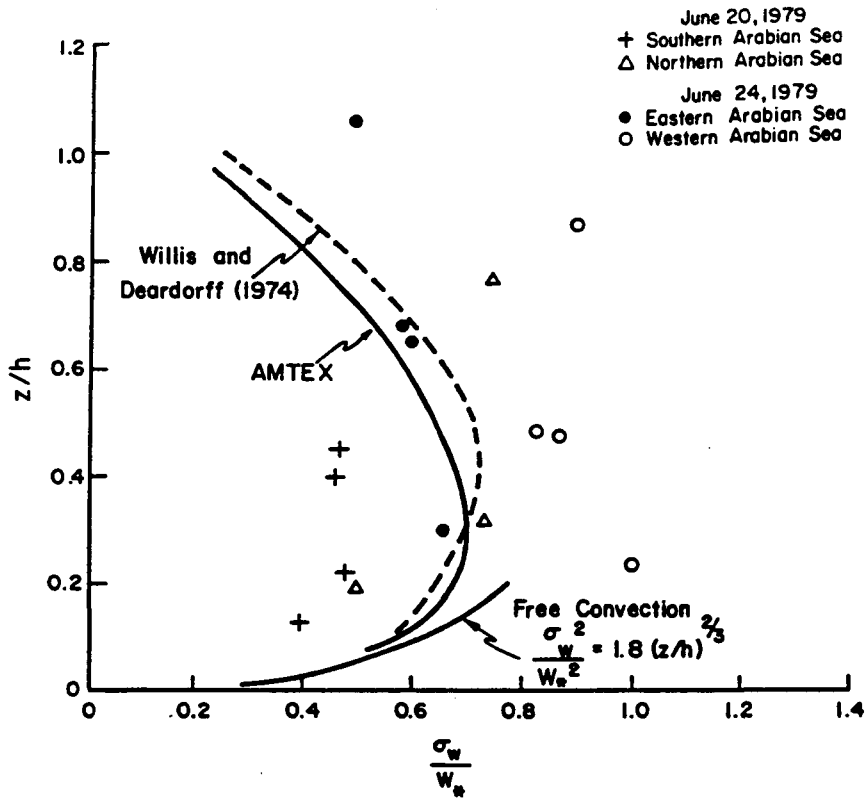

Fig. 6. Profile of standard deviation of vertical velocity σ_w normalized by w_* for both days over the Arabian Sea. Free convection curve is given along with Willis and Deardorff's (1974) curve from laboratory experiments. AMTEX curve is also given obtained from Lenschow *et al.* (1980).

Included are Willis and Deardorff's (1974) profile obtained from laboratory simulations, the Lenschow *et al.* (1980) profile from AMTEX data and the free convection prediction $\sigma_w^2/w_*^2 = 1.8(z/h)^{2/3}$ (Wyngaard *et al.*, 1971). Values of w_* along with other parameters for the Arabian Sea were given in Table I. Note in Figure 6 that σ_w/w_* data for the Western (○) and Northern (△) regions are generally greater than the Eastern (●) or Southern (+) regions. This could be expected from the observed mean temperature and wind profiles. The Western and Northern regions both show well-mixed near-neutral boundary layers with a stronger jet as opposed to a more shallow convective layer and slightly decreased wind speeds over the Eastern and Southern regions. Also note that the regions of larger convection (Northern and Western) have greater values of σ_w/w_* than those observed in AMTEX or by Willis and Deardorff (1974) while the values in the regions of decreased convection (Southern and Eastern) generally are smaller than AMTEX or Willis and Deardorff's values.

Figure 7 shows $\sigma_{u,v}$, the average of the standard deviations of u and v, normalized by w_* for both days along with Willis and Deardorff's (1974) laboratory results as in Figure 6. Obviously u, v turbulence values in the monsoon boundary layer over the Arabian Sea for this specific case are much larger than simulated in water-tank experiments in which the jet is not taken into account.

Panofsky *et al.* (1977) hypothesized from surface layer data that $\sigma_{u,v}$ could be approximated by:

$$\sigma_{u,v} = u_*(12 + h/|L|)^{1/3} . \tag{7}$$

Values obtained using this formulation for the four regions of the Arabian Sea are given in Table II. These values of $\sigma_{u,v}/w_*$ are in much better agreement with observed values shown in Figure 7.

TABLE II

$\sigma_{u,v}$ values (ms^{-1}) obtained from Panofsky *et al.* (1977) formulation for the Arabian Sea

Date	Region	$\sigma_{u,v}$	$\sigma_{u,v}/w_*$
20 June	Southern Arabian Sea	0.70	0.96
	Northern Arabian Sea	1.34	1.28
24 June	Western Arabian Sea	2.09	2.11
	Eastern Arabian Sea	0.85	1.19

The normalized temperature variance σ_T^2/θ_*^2 is given in Figure 8 along with free convection and laboratory curves. There is large scatter but all normalized observed values are greater than those predicted from free convection (range: 4–50 for

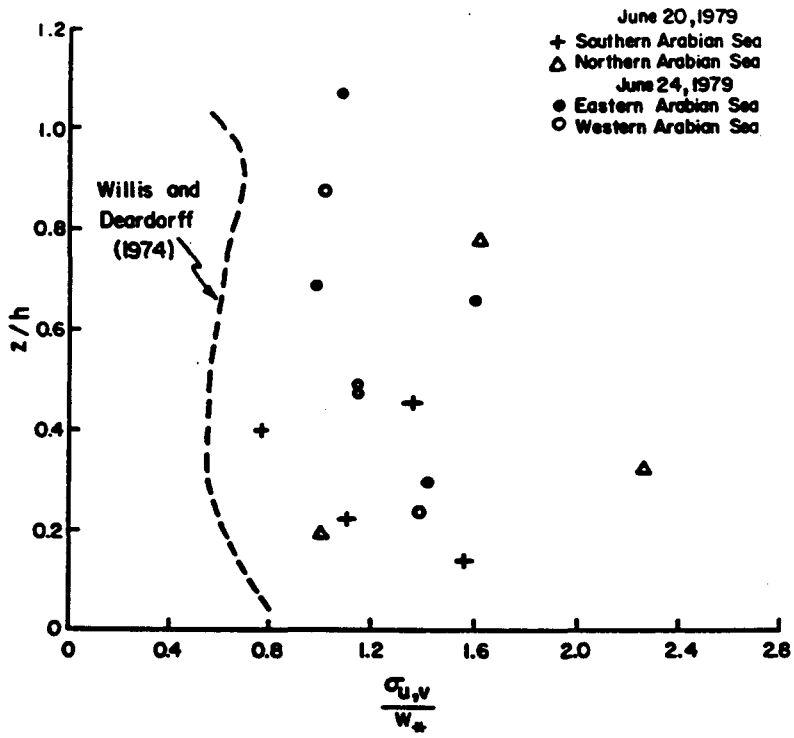

Fig. 7. Profile of the average of standard deviation of u and v velocity components $\sigma_{u,v}$ normalized by w_* for 20 and 24 June, 1979.

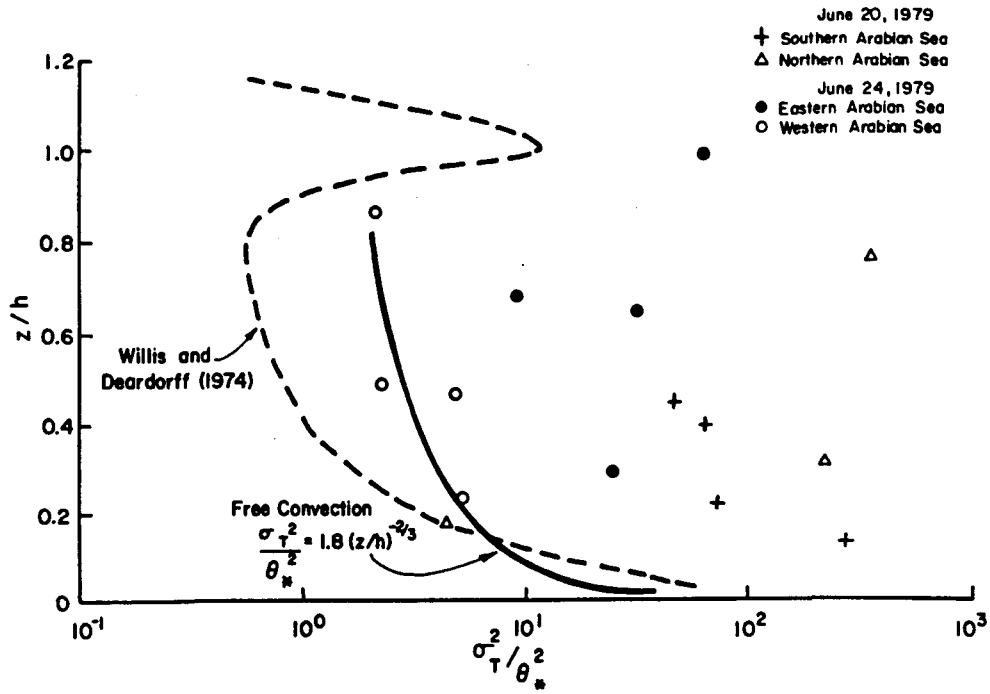

Fig. 8. Profile of temperature variance σ_T^2 normalized by θ_*^2 for both days over the Arabian Sea. Solid line is the free-convection prediction given by $\sigma_T^2/\theta_*^2 = 1.8(z/h)^{-2/3}$.

$0 < z/h \leq 1.0$) or laboratory experiments (range: 1–70 for $0 < z/h \leq 1.2$). The normalized variance is sensitive to the surface flux which could have been underestimated. Surface heat flux is a parameter difficult to estimate accurately. Notice that values of σ_T^2/θ_*^2 for 20 June (+, Δ) are generally larger than those of 24 June (●, ○). It is possible that the difference in the development of the monsoon flow for the two days could be an important factor. The low-level developing flow on 20 June obviously has different characteristics than the well-developed low-level flow on 24 June. As already mentioned, the interactions of the thermal structure and the jet structure in the monsoon boundary layer appear to be very important in determining turbulence variation. Differences in monsoonal flow and thus differences in the jet and thermal structure have an obvious effect on the σ_T^2 profile in Figure 8. The effect of clouds also appears to be an important factor. This is not yet completely understood because of lack of comprehensive data.

6. Turbulent Kinetic Energy Budget

The turbulent kinetic energy (TKE) budget in the boundary layer is given by:

$$\frac{\overline{\partial e'}}{\partial t} = \frac{g}{T_v}\,\overline{w'T_v'} - \frac{\tau}{\rho}\cdot\frac{\partial \mathbf{V}}{\partial z} - \frac{\partial}{\partial z}\left[\overline{w'e'} + \frac{\overline{w'p'}}{\rho}\right] - \varepsilon \tag{8}$$

where the kinetic energy $\overline{e'}$ is equal to $\frac{1}{2}(\overline{u'^2} + \overline{v'^2} + \overline{w'^2})$. The first term on the right-

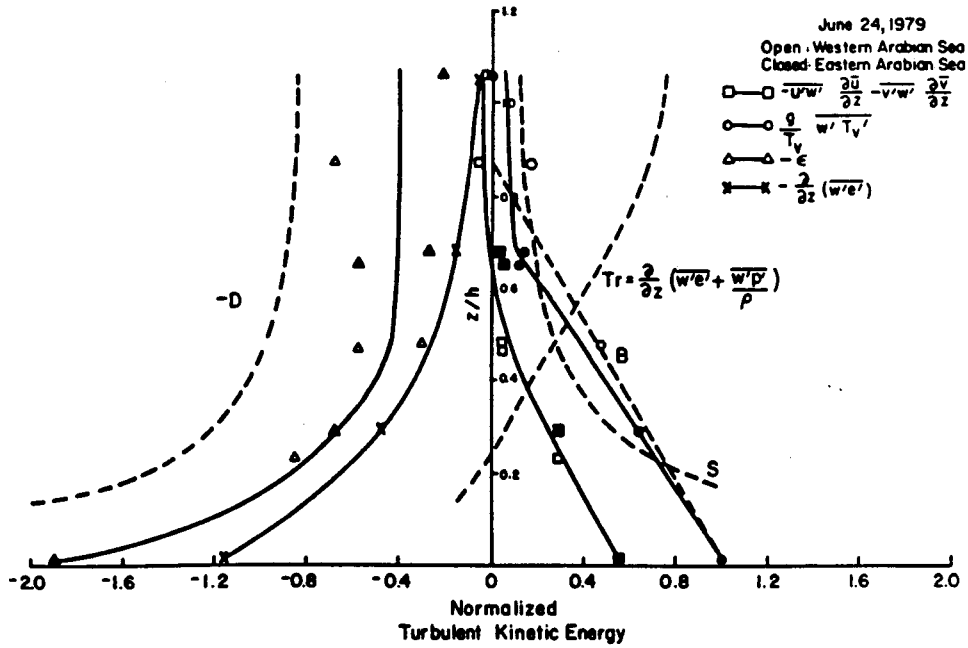

Fig. 9. Profile of turbulent kinetic energy budget normalized by surface heat flux for 24 June, 1979 over the Arabian Sea regions. Dashed lines represent theoretical curves obtained from Lenschow (1974) for buoyancy (B), shear (S), dissipation (D), and transport (Tr). Observed values given by solid lines are defined as: shear $-\overline{u'w'}\,\partial\bar{u}/\partial z - \overline{v'w'}\,\partial\bar{v}/\partial z$, (□); buoyancy $(g/T_v)\overline{w'T_v'}$, (○); dissipation ε, (△); and vertical turbulent transport $\partial/\partial z(\overline{w'e'})$, (×). Open symbols are for the Eastern region, closed symbols for the Western.

hand side, $g/T_v(\overline{w'T_v'})$ is the buoyancy term, the second $(\tau/\rho)\cdot(\partial \mathbf{V}/\partial z)$ is the shear term and the third $\partial/\partial z[\overline{w'e'} + (\overline{w'p'}/p)]$ is the turbulent transport term consisting of vertical and pressure transport. The fourth term ε is the dissipation of viscous energy. For the two observation days over the Arabian Sea, 20 June and 24 June, the time rate of change of kinetic energy $\overline{\partial e'}/\partial t$ was calculated to be approximately two orders of magnitude smaller than the other terms and is thus assumed negligible in the TKE budget.

Horizontal advection of kinetic energy $\bar{u}\,\overline{\partial e'}/\partial x$ is generally neglected in the surface layer (Lenschow, 1974). Calculations on 24 June in the boundary layer over the Arabian Sea using aircraft data indicate advection of kinetic energy to be on the order of $10^{-6}\ \mathrm{m^2\ s^{-3}}$ in the boundary layer, about three orders of magnitude smaller than the other terms. Thus, Equation (8) can be rewritten as:

$$\frac{g}{T_v}\,\overline{w'T_v'} - \left[\overline{u'w'}\,\frac{\partial\bar{u}}{\partial z} + \overline{v'w'}\,\frac{\partial\bar{v}}{\partial z}\right] - \frac{\partial}{\partial z}\left[\overline{w'e'} + \frac{\overline{w'p'}}{\rho}\right] - \varepsilon = 0\,. \qquad (9)$$

Lenschow (1974) proposed a model for the height variation of terms in the TKE budget based on aircraft measurements in the boundary layer. His model was for an unstably stratified barotropic planetary boundary layer over land. It is of interest here to use his model for this marine region to understand differences (or similarities) in the

two types of boundary layers. His formulation for the buoyancy (B) profile was based on observational evidence that heat flux is zero somewhere between $z/h = 0.85$ and 0.90. Thus,

$$B = 1 - 1.15\, z/h\,, \qquad 0 < z/h \leq 0.87\,. \tag{10}$$

Lenschow's normalized equations for shear (S) and dissipation (D) are as given below:

$$S = -\frac{L}{h}\left\{\frac{[1 - 15(h/L)z/h]^{-1/4}}{z/h}\right\} \tag{11}$$

$$D = 0.43 + \left\{\frac{0.57}{\langle S\rangle + 3.75}\,[\langle S\rangle - S]\right\} + S \tag{12}$$

where

$$\langle S\rangle = -\frac{L}{h}\left[\ln(h/z_0) - \left\{2\ln\left(\frac{1+x}{2}\right) + \ln\left(\frac{1+x^2}{2}\right) - 2\tan^{-1}x + \frac{\pi}{2}\right\}\right]$$

$$x = (1 - 15h/L)^{1/4}\,. \tag{13}$$

Transport (Tr) in Lenschow's model was calculated as a residual and includes both vertical and pressure transport.

Boundary-layer data obtained from aircraft, ships and dropwindsondes over the Arabian Sea were used as input in Lenschow's model. Parameters for Lenschow's equations, L and h were given in Table I. Roughness length z_0 was taken to be 0.001 m which is in agreement with values calculated from Charnock's relationship, $z_0 = \alpha u_*^2/g$ for the range of u_* over the Arabian Sea on 24 June. The value for α used is 0.014 (Garratt, 1977).

Figure 9 shows the TKE budget for 24 June over the Arabian Sea with all terms normalized by the surface heat flux $g/T_v(\overline{w'T_v'})_0$ plotted versus normalized height z/h. Observed values of shear (□), buoyancy (○), dissipation (△), and vertical transport (×) are given for both the Western Arabian Sea (represented by the open symbols □, ○, △) and the Eastern Arabian Sea (closed symbols ■, ●, ▲) with a solid line representing the average of both regions. Surface values estimated at 10 m for shear and buoyancy are calculated from bulk methods. Values of the viscous dissipation at 10 m are calculated from $\varepsilon = u_*^3/kz$. Pressure transport $\partial/\partial z(\overline{w'p'})$ is estimated as a residual.

It is interesting to note that when each term is normalized, there is not a large variation between the two regions. Dissipation shows the largest variation, from about -0.3 to -0.6 in the middle of the boundary layer. Although boundary-layer characteristics for the two regions over the Arabian Sea were different, as stated in Section 4, the budget of turbulent kinetic energy indicates that the magnitudes of sources and sinks appear comparable for both regions.

Buoyancy is the primary source term of kinetic energy in the monsoon boundary layer over the Arabian Sea. Figure 9 shows a near linear decrease with height of production

of turbulent kinetic energy with buoyancy approaching a value of zero at approximately $z = 0.85h$. Shear production also shows a near linear decrease with height, approaching zero at $z = 0.6h$.

Dissipation and turbulent transport are both important sink terms throughout the depth of the boundary layer over the Arabian Sea on 24 June. Dissipation approaches a constant value in the upper part of the boundary layer, as observed by others (LeMone, 1980; Lenschow, 1974). Turbulent transport ($\partial/\partial z(\overline{w'e'})$) over the Arabian Sea is a sink term throughout the boundary layer, approaching zero at $z = h$.

Also shown in Figure 9 are the model calculations (dotted lines) of buoyancy (B), shear (S), and dissipation (D) obtained from Lenschow's (1974) model of the turbulent kinetic energy budget mentioned earlier. The model calculation of buoyancy (dotted line B) is a close approximation to the observed profile throughout the boundary layer. Near the top of the boundary layer, the observed buoyancy profile approaches a finite value while the model profile goes to zero at $z = 0.87h$. The model formulation of shear, in which Lenschow assumed $\overline{u'w'}$ constant with height through the entire boundary layer, approximates the general shape of the observed shear profile in the upper part of the mixed layer but greatly overestimates near the surface. Overestimation is also observed in the model profile of dissipation. LeMone (1980) found this to be true for GATE data.

The difference between the solid line representing vertical turbulent transport ($\partial/\partial z(\overline{w'e'})$) and the dotted line for total transport ($\partial/\partial z(\overline{w'e'} + \overline{w'p'}/\rho)$) in Figure 9 approximates the relative size of pressure transport. It appears to be an important source term throughout the depth of the monsoon boundary layer over the Arabian Sea. Wyngaard and Coté (1971), McBean and Elliott (1975), Rayment and Caughey (1977), and Caughey and Wyngaard (1979) all suggested that pressure transport could be a significant term in the surface layer.

7. Conclusions

Observations of the mean and turbulence structure of the monsoon boundary layer over the central Arabian Sea during MONEX 79 were made from low-level NCAR Electra aircraft flights, ships and dropwindsondes. Results indicate the importance of the Somali Jet on both mean and turbulence structure. Indications of the northeastward advance of the monsoon are evident in differences between structures of the boundary layer from 20 June when the monsoon had just reached the observation region to 24 June when the southwest monsoon had totally covered the Arabian Sea. From mean profiles, regions in which the strong monsoon flow is not as evident (20 June, Southern Arabian Sea region and 24 June, Eastern Arabian Sea region) show much more stable boundary-layer conditions with an elevated jet situated roughly at the height of the strong capping inversion. Regions in which there existed a more well-mixed layer near the surface up to 1000 m (20 June Northern region and 24 June Western region) were generally associated with more cumulus activity and showed a jet structure depressed in height.

Flux and turbulence profiles show differences from profiles presented in the literature for fair weather tropical or trade-wind boundary layers. Turbulence data of horizontal wind components u and v both show values much larger than those observed in laboratory experiments or in tropical boundary layers in which the strong jet was not present. Vertical velocity turbulence (σ_w) for conditions in which strong low-level monsoon flow was observed is typically larger than AMTEX or laboratory results.

The turbulent kinetic energy budget over the Arabian Sea on 24 June shows similar results for both the Eastern and Western observation regions. Buoyancy is the primary source of kinetic energy. However, in comparison to a typical monsoon boundary over the Bay of Bengal (Holt and Raman, 1986), both buoyancy and shear are important production terms through a greater depth of the boundary layer. Buoyancy approaches zero at a height approximately $z = 0.85h$, shear at a height $z = 0.6h$. The increased shear over the Arabian Sea in comparison to the Bay of Bengal is probably due to the presence of the low level jet. Values of $\overline{w' T_v'}$ over the more convective regions of the Arabian Sea studied here are approximately three to five times larger than the values observed over the Bay of Bengal (Holt and Raman, 1986).

Acknowledgment

This work was supported by the Global Atmospheric Research Program of the National Science Foundation under the grant ATM–82–17960.

References

Bannon, P. R.: 1982, 'On the Dynamics of the East African Jet. III: Arabian Sea Branch', *J. Atmos. Sci.* **39**, 2267–2278.

Barnes, S. L.: 1968, 'An Empirical Shortcut to the Calculation of Temperature and Pressure at the Lifted Condensation Level', *J. Appl. Meteorol.* **7**, 511.

Bolhofer, W., Chambers, M., Frey, D., Kuettner, J., and Unninayar, S.: 1981, Summer MONEX US Research Flight Missions, May–July 1979, NCAR Technical Note, NCAR/TN-168 + STR.

Cadet, D. and Reverdin, G.: 1981, 'Water Vapour Transport over the Indian Ocean During Summer 1975', *Tellus* **33**, 476–487.

Caughey, S. J. and Wyngaard, J. C.: 1979, 'The Turbulence Kinetic Energy Budget in Convective Conditions', *Quart. J. Roy. Meteorol. Soc.* **105**, 231–239.

Findlater, J.: 1977, 'Observational Aspects of the Low Level Cross Equatorial Jet Stream', in T. N. Krishnamurti (ed.), *Monsoon Dynamics*, Birkhauser Verlag, Basel, Stuttgart, pp. 1251–1262.

Findlater, J.: 1969, 'A Major Low-Level Air Current near the Indian Ocean During the Northern Summer', *Quart. J. Roy. Meteorol. Soc.* **95**, 362–380.

Garratt, J. R.: 1977, 'Review of Drag Coefficients over Oceans and Continents', *Mon. Wea. Rev.* **105**, 915–929.

Grossman, R. L. and Durran, D. R.: 1984, 'Interaction of Low-Level Flow with the Western Ghat Mountains and Offshore Convection in the Summer Monsoon', *Mon. Wea. Rev.* **112**, 652–672.

Holt, T. and SethuRaman, S.: 1985, 'Aircraft and Ship Observations of the Mean, Structure of the Marine Boundary Layer over the Arabian Sea During MONEX 79, *Boundary-Layer Meteorol.* **33**, 259–282.

Holt, T. and Raman, S.: 1986, 'Observations of the Mean and Turbulence Structure of the Marine Boundary Layer over the Bay of Bengal During MONEX 79', *Mon. Wea. Rev.* (in press).

LeMone, M. A.: 1980, 'The Marine Boundary Layer', *Workshop on the Planetary Boundary Layer*, Amer. Meteorol. Soc., Boston, MA, 182–246.

Lenschow, D. H., Wyngaard, J. C., and Pennell, W. T.: 1980, Mean-Field and Second-Moment Budgets in a Baroclinic, Convective Boundary Layer', *J. Atmos. Sci.* **37**, 1313–1326.

Lenschow, D. H.: 1974, 'Model of the Height Variation of the Turbulence Kinetic Energy Budget in the Unstable Planetary Boundary Layer', *J. Atmos. Sci.* **31**, 465–474.

McBean, G. A. and Elliot, H. A.: 1975, 'The Vertical Transports of Kinetic Energy by Turbulence and Pressure in the Boundary Layer', *J. Atmos. Sci.* **37**, 753–766.

Nicholls, S. and LeMone, M. A.: 1980, 'The Fair Weather Boundary Layer in GATE: The Relationship of Subcloud Fluxes and Structure to the Distribution and Enhancement of Cumulus Clouds', *J. Atmos. Sci.* **37**, 2051–2067.

Panofsky, H. A., Tennekes, H., Lenschow, D. H., and Wyngaard, J. C.: 1977, 'The Characteristics of Turbulent Velocity Components in the Surface Layer under Convective Conditions', *Boundary-Layer Meteorol.* **11**, 355–361.

Rayment, R. and Caughey, S. J.: 1977, 'An Investigation of the Turbulence Balance Equations in the Atmospheric Boundary Layer', *Boundary-Layer Meteorol.* **11**, 15–26.

Saha, K. R. and Bavadekar, S. N.: 1973, 'Water Vapour Budget and Precipitation over the Arabian Sea During the Northern Summer', *Quart. J. Roy. Meteorol. Soc.* **99**, 273–278.

Sikka, D. R. and Grossman, R. L.: 1980, *Summar MONEX Chronological Weather Summary*, International MONEX Management Centre, New Delhi, India, December 1980 (first edition), 49 pp.

van de Boogaard, H. and Rao, G. V.: 1984, 'Mesoscale Structure of the Low-Level Flow near the Equatorial East African Coast', *Mon. Wea. Rev.* **112**, 91–107.

Willis, G. E. and Deardorff, J. W.: 1974, 'A Laboratory Model of the Unstable Planetary Boundary Layer', *J. Atmos. Sci.* **31**, 1297–1307.

Wyngaard, J. C. and Coté, O. R.: 1971, 'The Budgets of Turbulent Kinetic Energy and Temperature Variance in the Atmospheric Surface Layer', *J. Atmos. Sci.* **28**, 190–201.

Wyngaard, J. C., Coté, O. R., and Izumi, Y.: 1971, 'Local Free Convection, Similarity and the Budgets of Shear and Heat Flux', *J. Atmos. Sci.* **28**, 1171–1182.